Quantum Spin-Valley Hall Kink States: From Concept to Materials Design

Tong Zhou, Shuguang Cheng, Michael Schleenvoigt, Peter Schüffelgen, Hua Jiang, Zhongqin Yang, and Igor Žutić

Phys. Rev. Lett. **127**, 116402 — Published 9 September 2021

DOI: 10.1103/PhysRevLett.127.116402

Quantum Spin-Valley Hall Kink States: From Concept to Material Design

Tong Zhou,[1,*] Shuguang Cheng,[2] Michael Schleenvoigt,[3] Peter Schüffelgen,[3] Hua Jiang,[4] Zhongqin Yang,[5] and Igor Žutić[1,†]

[1]*Department of Physics, University at Buffalo, State University of New York, Buffalo, New York 14260, USA*
[2]*Department of Physics, Northwest University, Xi'an 710069, China*
[3]*Peter Grünberg Institute 9, Forschungszentrum Jülich & JARA Jülich-Aachen Research Alliance, 52425 Jülich, Germany*
[4]*School of Physical Science and Technology, Soochow University, Suzhou 215006, China*
[5]*State Key Laboratory of Surface Physics and Key Laboratory of Computational Physical Sciences (MOE) and Department of Physics and Collaborative Innovation Center of Advanced Microstructures, Fudan University, Shanghai 200433, China*

(Dated: August 13, 2021)

We propose a general and tunable platform to realize high-density arrays of quantum spin-valley Hall kink (QSVHK) states with spin-valley-momentum locking based on a two-dimensional hexagonal topological insulator. Through the analysis of Berry curvature and topological charge, the QSVHK states are found to be topologically protected by the valley-inversion and time-reversal symmetries. Remarkably, the conductance of QSVHK states remains quantized against both nonmagnetic short/long-range and magnetic long-range disorder, verified by the Green function calculations. Based on first-principles results and our fabricated samples, we show that QSVHK states, protected with a gap up to 287 meV, can be realized in bismuthene by alloy engineering, surface functionalization, or electric field, supporting non-volatile applications of spin-valley filters, valves, and waveguides even at room temperature.

Two-dimensional (2D) hexagonal lattices offer a versatile platform to manipulate charge, spin, and valley degrees freedom and implement different topological states. While pioneering predictions for quantum anomalous and quantum spin Hall (QSH) effect [1, 2] were guided by graphene-like systems, graphene poses inherent difficulties with its weak spin-orbit coupling (SOC) and a gap of only $\Delta \sim 40\,\mu$eV [3]. The quest for different 2D hexagonal monolayers (MLs) with a stronger SOC on one hand reveals, as in transition metal dichalcogenides (TMDs), an improved control of valley-dependent phenomena [4], emulating extensive research in spintronics [5], while on the other hand, as in ML Bi on SiC substrate, topological states remain even above the room temperature, with a huge topological gap ~ 0.8 eV [6]. However, examples where valley degrees of freedom support robust topological states are scarce.

In 2D materials with broken inversion symmetry, such as gapped graphene [7–12] and TMDs [13, 14], the opposite sign of the momentum-space Berry curvature $\mathbf{\Omega}(\mathbf{k})$ in different valleys is responsible for a valley Hall effect, where the carriers in different valleys turn into opposite directions transverse to an in-plane electric field [7, 14]. A striking example of such a sign reversal in $\mathbf{\Omega}(\mathbf{k})$ along an internal boundary of a film is realized in quantum valley Hall kink (QVHK) states [15–29]. The resulting topological defect supports counterpropagating 1D chiral electrons, topologically protected by the valley-inversion symmetry [15–19]. The underlying mechanism for the formation of zero-energy states, expected from the index theorem [30, 31], shares similarities with many other systems in condensed matter and particle physics [32–39]. While the proposals for QVHK mainly focus on bilayer graphene (BLG) systems [20–24], the required sign reversal in $\mathbf{\Omega}(\mathbf{k})$ realized by either the random local stacking faults [20, 22], or a dual-split-gate structure [21, 23, 24], is challenging to implement to achieve high-density channels. With the required applied electric field, the volatility of QVHK limits their envisioned use in valleytronics. A small gap of BLG ~ 20 meV [21] excludes high-temperature applications, and QVHK states were limited to 5 K [20–24]. Crucially, disorder easily induces intervalley scattering, preventing the expected ballistic transport in QVHK states [20, 21, 29].

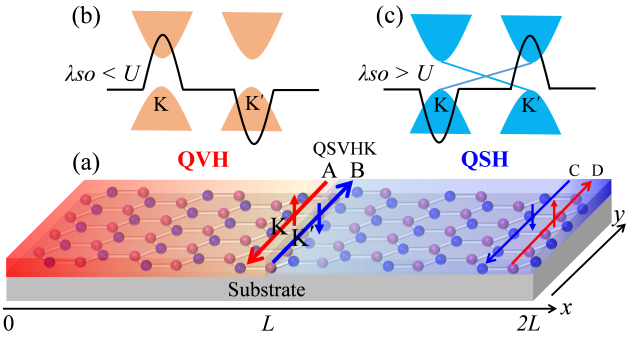

FIG. 1. (a) Schematic of the QSVHK states (A, B) at the valleys K and K', and QSH edge states (C, D) in a junction formed by QVH and QSH insulators. $2L$ is the junction length. The red (blue) arrow denotes the spin-up (down) channel. (b) and (c) the schematic of the bands and Berry curvatures (black lines) for QVH and QSH insulators, distinguished by the relative strength of SOC, λ_{SO}, and staggered potential, U.

Motivated by these challenges, we propose a robust platform to realize high-density arrays of spin-polarized QVHK states at room temperature based on a 2D hexagonal topological insulator, where the QVHK states are simultaneously the QSH edge states, forming along the QSH-QVH interface as shown in Fig. 1. The QSH is described by a topological invariant $Z_2 = 1$ [2], while the QVH is characterized by a quantized valley Chern number $C_V = 1$ and $Z_2 = 0$ [8, 19]. Across their interface, both Z_2 and C_V change the value, thus the QSH and QVHK states simultaneously emerge along the interface, giving largely unexplored topological kink states, we term quantum spin-valley Hall kink (QSVHK) states. Unlike the pre-

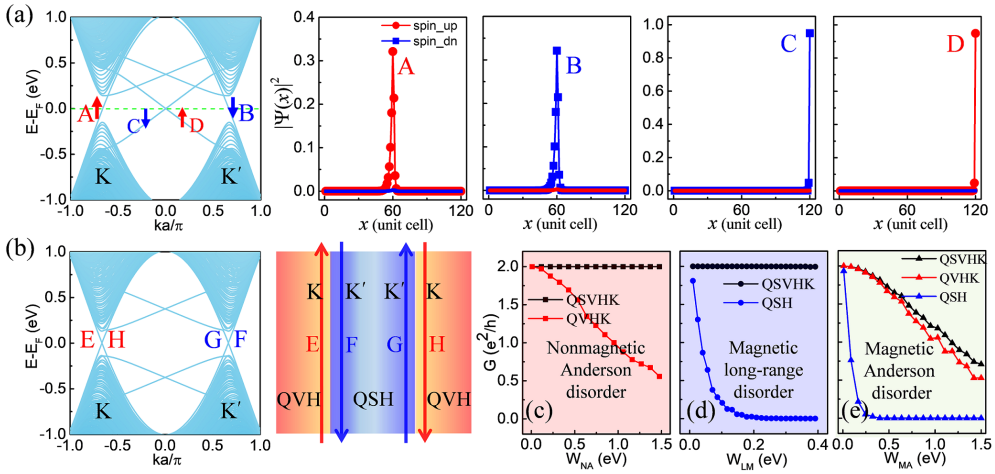

FIG. 2. (a) Bands and wave function distributions ($|\Psi(x)|^2$) for topological states A-D in the QSH-QVH junction with $L = 60$ unit cells. (b) Bands and schematic of QVH-QSH-QVH junction with pure QSVHK states E-H. (c) Junction conductance,G, versus nonmagnetic Anderson disorder strength W_{NA} at the Fermi level, for the QSVHK and QVHK. (d) Same as (c) but for the QSVHK and QSH versus magnetic long-range disorder strength W_{LM}. (e) Same as (c) but versus magnetic Anderson disorder strength W_{MA}. The parameters U, λ_{SO} for QVH and QSH regions are taken from the BiAs/SiC and Bi/SiC, respectively. The hopping parameter $t_{1,2} = 1$ eV.

vious studies of the interplay between topological states [15–29, 36–46], our proposed QSVHK shows a peculiar marriage between QSH and QVH. The QSH becomes robust against the magnetic long-range disorder due to the valley-inversion symmetry protection of the QVH [15–19], while the QVH can be robust against the nonmagnetic short-range disorder because of the time-reversal symmetry protection of the QSH [2, 47]. Thus, in contrast to the trivial spin-valley Hall effects [48–50], the topological QSVHK states are robust against both nonmagnetic short/long-range and magnetic long-range disorder, giving robust ballistic spin-valley-momentum locking transport. The QSH-QVH junction can be implemented by inducing a staggered potential, U, in a part of the 2D topological insulators. When U is smaller (larger) than the strength of the intrinsic SOC, λ_{SO}, the QSH (QVH) is obtained. Our first-principles calculations reveal that U can be induced by alloy engineering or surface decoration and easily controlled by the electric filed.

We first present our idea through the analysis of a tight-binding model based on p_x and p_y orbitals, which is widely used to describe the physics of the hexagonal MLs including arsenene [51, 52], antimonene [41, 42, 53, 54], bismuthene [6, 50, 55], and binary element group-V MLs [56, 57]

$$H = \lambda_{SO}\sum_i c_i^+\sigma_z\otimes s_z c_i + \sum_i U_i c_i^+\sigma_0\otimes s_0 c_i + \left(\sum_i\sum_{j=1,2,3} c_i^+ T_{\delta_j} c_{i+\delta_j} + H.C.\right). \quad (1)$$

Here, c_i represents the annihilation operator on site i. σ and s indicate the Pauli matrices acting on orbital and spin spaces. The first term describes the intrinsic SOC and the second term gives the staggered potential with $U_i = U(-U)$ for the $A(B)$ sublattice. The hopping term

$$T_{\delta_j} = \begin{bmatrix} t_1 & z^{(3-j)}t_2 \\ z^j t_2 & t_1 \end{bmatrix}\otimes s_0, \quad (2)$$

describes the nearest hopping from site i to $i+\delta_j$, where z=exp($2i\pi/3$) and $t_{1/2}$ is the hopping coefficient. In the absence of the first two terms in Eq. (1), the gapless Dirac points exist at the two valleys [50, 55]. The staggered potential and intrinsic SOC open a gap of $2|\lambda_{SO} - \mathrm{U}|$ at the Dirac points and their competition determines the topology of the system. When $\lambda_{SO} < U$, the system is in QVH with $Z_2 = 0$ and opposite $\mathbf{\Omega}(\mathbf{k}) \neq 0$ at the two valleys [Fig. 1(b)]. When $\lambda_{SO} > U$, the system is in QSH with $Z_2 = 1$ and for $U > 0$ the sgn[$\mathbf{\Omega}(\mathbf{k})$] is reversed as compared to the QVH [Fig. 1(c)]. We consider a planar junction formed by the QVH and QSH [Fig. 1(a)], where QSVHK emerges along their interface, since both Z_2 and $\mathbf{\Omega}(\mathbf{k})$ change the sign.

To identify such QSVHK states, we calculate the spectrum of the QSH-QVH junction along the zigzag direction, where the valley degree can be preserved [29, 58, 59]. As shown in Fig. 2(a), there are four non-degenerate gapless states, $A-D$, in the bulk band gap. The helical C and D states are the common QSH states localized at the outer edge of the QSH region, verified by their wave functions in Fig. 2(a). The A (B) state at the K (K') valley shows the QSVHK localized at the inner interface [Fig. 2(a)]. Unlike the QVHK in BLG, the QSVHK is fully spin-polarized. Specifically, the kink state A (B) at K (K') valley has spin-up (down) channel. Such spin-valley-momentum locking supports a perfect spin-valley filter.

To better understand the emergence of the QSVHK, we focus on the low-energy physics of Eq.(1). We expand the Hamiltonian around the valleys and obtain a continuum model

$$H = \hbar v_F\left(k_x\sigma_x + \tau_z k_y\sigma_y\right) + \lambda_{SO}s_z\tau_z\sigma_z + U\sigma_z, \quad (3)$$

where v_F is the Fermi velocity, σ, s, and τ are Pauli matrix for orbital, spin, and valley, respectively. From the index theorem [30], the number of the kink channels is related to the change of the bulk topological charges across the interface [15, 19, 60]. The spin- and valley-projected topological charge $C_{\tau_z}^{s_z}$ can be calculated by integrating the spin-dependent $\mathbf{\Omega}(\mathbf{k})$ of the valence bands around each valley [15, 19, 60]. From the continuum model in Eq. (3), we obtain

$$C_{\tau_z}^{s_z} = \frac{\tau_z}{2}\,\mathrm{sgn}\left(U - \tau_z s_z \lambda_{SO}\right). \tag{4}$$

In the QVH region, we get $\left(C_K^{\uparrow}, C_K^{\downarrow}, C_{K'}^{\uparrow}, C_{K'}^{\downarrow}\right)$ = (0.5, 0.5, -0.5, -0.5), while in the QSH region, $\left(C_K^{\uparrow}, C_K^{\downarrow}, C_{K'}^{\uparrow}, C_{K'}^{\downarrow}\right)$ = (-0.5, 0.5, -0.5, 0.5). The number of the kink modes per spin/valley $\left(\nu_K^{\uparrow}, \nu_K^{\downarrow}, \nu_{K'}^{\uparrow}, \nu_{K'}^{\downarrow}\right)$ is an integer evaluated from the difference between the topological charges in two regions [15, 19], i.e., $\left(\nu_K^{\uparrow}, \nu_K^{\downarrow}, \nu_{K'}^{\uparrow}, \nu_{K'}^{\downarrow}\right)$ = (1, 0, 0, -1). It is clear the spin-up (down) topological charge has an integer change at the K (K') valley, giving the spin-valley polarized QSVHK. This topological charge analysis is consistent with our discussion about the energy spectrum in Fig. 2(a). In QSH-QVH junctions, there are still QSH states along the outer edge. To eliminate them and realize a pure QSVHK transport, we propose in Fig. 2(b) a QVH-QSH-QVH junction, where the two pairs of QSVHK are verified by the calculated bands. Multiple channels can be expected with more QSH-QVH boundaries, where the width of each region should be large enough to avoid the interplay between adjacent QSVHK states.

For valley-related transport, the influence of the short-(long)-range disorder is usually significantly different since the former (later) induces (excludes) intervalley scattering [61]. The former (later) is characterized by the smaller (larger) disorder correlation length, λ, compared to the lattice spacing, a [61]. For example, the QVHK is only robust against the long-range disorder [15–24]. To explore the robustness of the QSVHK against the disorder, we calculate the junction conductance, G, using the Landauer-Büttiker formula [62] and the Green-function method [63–66] in the presence of nonmagnetic Anderson disorder ($\lambda \to 0$) [64, 67] in the energy range (-W_{NA}/2, W_{NA}/2), magnetic Anderson disorder [65, 68] (-W_{MA}/2, W_{MA}/2), and magnetic long-range ($\lambda = 7a$) disorder [69, 70] (-W_{LM}/2, W_{LM}/2), where W_{NA}, W_{MA}, and W_{LM} measure their respective strengths. For comparison, we calculate $G(W_{NA})$, $G(W_{LM})$ and $G(W_{MA})$ in QVHK and QSH states, shown in Figs. 2(c)-(e). See calculation details and the crossover between the short- and long-range disorder in Supplemental Material (SM) [71]. For the QVHK with valley-momentum locking, its G decreases with W_{NA} increases, consistent with previous studies [20, 21], because the Anderson disorder breaks the valley-inversion symmetry and leads to the intervalley scattering. For QSH with spin-momentum locking, its G decreases with W_{LM} (W_{MA}), because the time-reversal symmetry is broken by the magnetic disorder, in agreement with the experiments [80, 81]. In contrast, for QSVHK with spin-valley-momentum locking protected by both valley-inversion and time-reversal symmetries, its G remains quantized against both nonmagnetic Anderson disorder and magnetic long-range disorder [Figs. 2(c)-(d)]. The backscattering in QSVHK can only be induced by simultaneously breaking the valley-inversion and time-reversal symmetries, for example by magnetic Anderson disorder [Fig. 2(e)]. However, with W_{MA}, the G of QSVHK is still higher than that of the QSH and QVH, since simultaneously scattering spin and valley is harder than scattering each of them.

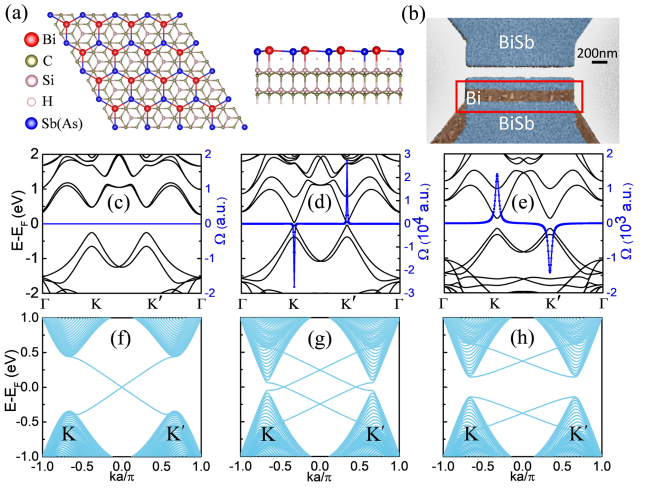

FIG. 3. (a) Top and side views of a ML BiSb or BiAs on a SiC substrate. (b) Scanning electron micrograph image of the planar BiSb-Bi-BiSb junction with a Si_3N_4 stencil mask (grey) 300 nm above the film for shadowing. BiSb-Bi interfaces are marked by the red rectangle. (c)-(e) Bands (black) and Berry curvatures, $\mathbf{\Omega}(\mathbf{k})$ (blue), of the valence bands for the Bi/SiC, BiSb/SiC, and BiAs/SiC, respectively. (f)-(h) Bands of the zigzag nanoribbons for the Bi/SiC, BiSb/SiC, and BiAs/SiC, respectively. The fitted parameters (λ_{SO}, U) for Bi/SiC, BiSb/SiC, and BiAs/SiC are (0.44 eV, 0 eV), (0.30 eV, 0.26 eV), and (0.24 eV, 0.38 eV), respectively.

Material design. The key factor to achieve QSVHK is creating an interface of the QSH and QVH. Since there are large number of hexagonal QSH insulators [58], a natural way to obtain such an interface is to engineer a part of QSH insulator into a QVH region, where $U > \lambda_{SO}$ is required. Recently, group-V MLs bismuthene, antimonene, and arsenene on a SiC substrate were predicted to be high-temperature 2D topological insulators [82]. For Bi/SiC, a huge nontrivial gap of 0.8 eV has been measured [6], originating from the intrinsic SOC of Bi $p_{x,y}$ orbitals [71]. However, with its inversion symmetry, Bi/SiC fails to show valley-dependent effects, as verified by $\mathbf{\Omega}(\mathbf{k}) = \mathbf{0}$ at all $\mathbf{k}$ [Fig. 3(c)]. To break the inversion symmetry, we propose to use alloy engineering to induce U in bismuthene, a well-established approach to tailor electronic and topological properties [83, 84]. Specifically, we propose to grow binary group-V MLs BiSb or BiAs on the SiC substrate, depicted in Fig. 3(a). We expect the change in the binary composition alters the strength of SOC (growing with the atomic number Z) and U (growing with a relative difference in Z of the two group-V elements), thus favoring either QVH or QSH insulators, as shown in Fig. 1(a). BiSb

and BiAs films can be fabricated using molecular beam epitaxy (MBE) [Fig. 3(b)], similar to that growth of Bi/SiC or exfoliated from bulk [51, 52]. From first-principles calculations, we see the BiSb/SiC and BiAs/SiC bands near E_F can be accurately described by the Hamiltonian in Eq. (1) [71].

Without considering SOC, Bi/SiC has gapless Dirac bands at two valleys, while the trivial gaps of 0.52 eV and 0.76 eV are opened in BiSb/SiC and BiAs/SiC [71], respectively. Such gaps, originating from the staggered potential, give $U_{\mathrm{BiSb/SiC}}$ = 0.26 eV and $U_{\mathrm{BiAs/SiC}}$ = 0.38 eV. With SOC, a nontrivial gap of 66 meV is opened in BiSb/SiC with $\mathbf{\Omega}(\mathbf{k}) \neq \mathbf{0}$ [Fig. 3(d)], giving a QSH insulator with $Z_2 = 1$ and the helical edge states [Fig. 3(g)]. The edge states outside the gap are not useful for the robust dissipationless transport, because they are negligible compared to the huge contribution from the trivial bulk bands [47]. Figure 3(e) reveals a different situation for BiAs/SiC. Due to $U > \lambda_{SO}$, a gap of 287 meV appears at K and K' with $Z_2 = 0$ and no topological edge states [Fig. 3(h)]. Compared to BiSb/SiC, the sign reversal of $\mathbf{\Omega}(\mathbf{k})$ for BiAs/SiC gives the desired QVH phase.

The resulting QSH-QVH junction [Fig. 1] can be realized combining BiAs/SiC (QVH) with Bi/SiC (QSH) or BiSb/SiC (QSH). Alternatively, to simplify the fabrication and yield QSH with an even larger nontrivial gap, BiAs-Bi/SiC junction is desirable, where the verified QSVHK states are shown in Fig. 2(a). In this analysis we exclude Rashba SOC [5], since its influence is negligible in QSVHK as discussed in the SM [71]. The BiAs-Bi/SiC junction provides a robust platform for QSVHK, protected by a global gap of 287 meV, which is ∼ 14 times larger than in BLG [21], supporting ballistic transport at high temperatures, verified by the finite-temperature Green-function calculations and dicussion about the influence of the many-body interaction [71].

The desired QSH-QVH junction can be fabricated using our well-established MBE selective area growth and stencil lithography [85] as shown in Fig. 3(b). The fabrication process and the influence of the stoichiometry are demonstrated in [71]. Multiple QSH-QVH boundaries can be created by spatially-selective deposition [85, 86], enabling transport of high-density channels. QSVHK robust against nonmagnetic and long-range disorder and insensitive to the interface configurations [71], facilitates its experimental observation and possible applications. Unlike QVHK in BLG, the QSVHK in bismuthene is spin-polarized and requires no external field. This offers non-volatility in unexplored applications coupling spin and valley, going beyond low-temperature BLG valleytronic applications [23]. For example, QSVHK supports fully spin-polarized quantum valley currents, making spin-valley filters, valves, and waveguides possible, or extend the fuctionalities for spin interconnects [87–89].

Another way to realize QSVHK in bismuthene system is surface decoration, widely used to modify the properties of the 2D materials [90]. Particularly, hydrogenation and halogenation have been a powerful tool to induce large-gap QSH states in group-IV and V MLs [55, 91]. Based on first-principles calculations, we show in Fig. 4 that the λ_{SO} and U in MLs BiAs

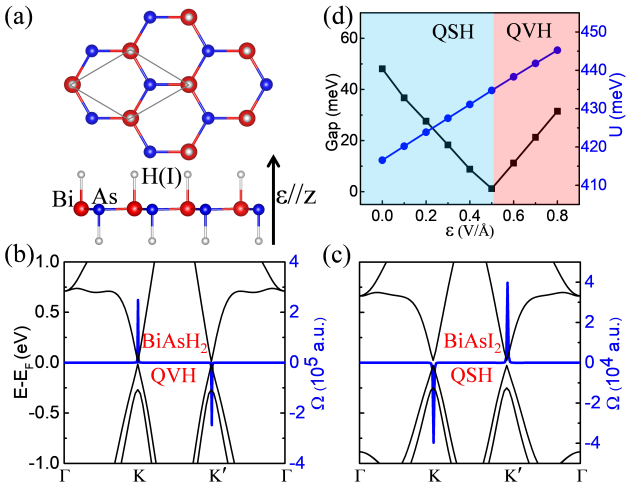

FIG. 4. (a) Top and side views of the MLs $BiAsH_2$ or $BiAsI_2$. (b) and (c) Bands (black) with Berry curvatures (blue) for MLs $BiAsH_2$ and $BiAsI_2$. (d) Electric-field dependent gap in a ML $BiAsI_2$.

can be tuned by the surface decoration, giving either a QSH or a QVH insulator. The structure of the hydrogenated ($BiAsH_2$) and halogenated ($BiAsI_2$) BiAs MLs are shown in Fig. 4(a). From the calculated bands and $\mathbf{\Omega}(\mathbf{k})$ in Figs. 4(b) and (c), we see the desired difference between $BiAsH_2$ and $BiAsI_2$. While the first is a QVH insulator with a trivial gap of 26 meV, $Z_2 = 0$, and $\mathbf{\Omega}(\mathbf{k}) \neq \mathbf{0}$ at K and K', the second $BiAsI_2$ is a QSH insulator with a nontrivial gap of 49 meV, $Z_2 = 1$, and reversed $\mathbf{\Omega}(\mathbf{k})$. When such two MLs form a junction [Fig. 1], the QSVHK can emerge along its interface. With hydrogenated and halogenated graphene routinely fabricated [92, 93], the $BiAsH_2$-$BiAsI_2$ junction could be obtained from ML BiAs to support QSVHK by using the spatially-selective growth and stencil lithography [71]. Since the electric field, ε, can directly change U in 2D materials [21, 23], we also explore the possibility of ε-controlled QSVHK. Figure 4(d) shows that for ε applied along the z direction in ML $BiAsI_2$, U is increased and the gap is closed when $\varepsilon = 0.5$ $V/$Å, the value achievable with ion-liquid gating [94, 95]. Such a gap closing indicates a topological transition from QSH to QVH. Thus, the electric field can also be used to generate and control the QSVHK.

With experimental realization of the QSVHK it would be possible to verify their inherent robustness of quantized conductance of spin-polarized channels, in contrast to QSH insulators, where this quantization is fragile even at He temperatures [80, 81]. Furthermore, QSVHK offers an intriguing opportunity to study its manifestations of topological superconductivity through proximity effects [81, 88, 96] and test the related role of disorder [97, 98].

We thank Prof. Fan Zhang for fruitful discussions. This work is supported by the U.S. DOE, Office of Science BES, Award No. DE-SC0004890 (T. Z. and I. Ž.), NSFC under Grant Nos. 11874298 (S. C.), 11822407 (H. J.), 11874117 (Z. Y.), and 11574051 (Z. Y.), German Federal Ministry of Education and Research (BMBF) via the Quantum Futur project

"MajoranaChips" (Grant No. 13N15264) within the funding program Photonic Research Germany (M. S. and P. S.) and the UB Center for Computational Research.

* tzhou8@buffalo.edu
† zigor@buffalo.edu

[1] F. D. M. Haldane, Model for a Quantum Hall Effect without Landau Levels: Condensed-Matter Realization of the "Parity Anomaly", Phys. Rev. Lett. **61**, 2015 (1988).
[2] C. L. Kane and E. J. Mele, Z_2 Topological Order and the Quantum Spin Hall Effect, Phys. Rev. Lett. **95**, 146802 (2005).
[3] J. Sichau, M. Prada, T. Anlauf, T. J. Lyon, B. Bosnjak, L. Tiemann, and R. H. Blick, Resonance Microwave Measurements of an Intrinsic Spin-Orbit Coupling Gap in Graphene: A Possible Indication of a Topological State, Phys. Rev. Lett. **122**, 046403 (2019).
[4] X. Xu, W. Yao, D. Xiao, and T. F. Heinz, Spin and pseudospins in layered transition metal dichalcogenides, Nat. Phys. **10**, 343 (2014).
[5] I. Žutić, J. Fabian, and S. Das Sarma, Spintronics: Fundamentals and applications, Rev. Mod. Phys. **76**, 323 (2004).
[6] F. Reis, G. Li, L. Dudy, M. Bauernfeind, S. Glass, W. Hanke, R. Thomale, J. Schäfer, and R. Claessen, Bismuthene on a SiC substrate: A candidate for a high-temperature quantum spin Hall material, Science **357**, 287 (2017).
[7] D. Xiao, W. Yao, and Q. Niu, Valley-Contrasting Physics in Graphene: Magnetic Moment and Topological Transport, Phys. Rev. Lett. **99**, 236809 (2007).
[8] Z. Qiao, W.-K. Tse, H. Jiang, Y. Yao, and Q. Niu, Two-dimensional Topological Insulator State and Topological Phase Transition in Bilayer Graphene, Phys. Rev. Lett. **107**, 256801 (2011).
[9] E. McCann and M. Koshino, The electronic properties of bilayer graphene, Rep. Prog. Phys. **76**, 056503 (2013).
[10] R. V. Gorbachev, J. C. W. Song, G. L. Yu, A. V. Kretinin, F. Withers, Y. Cao, A. Mishchenko, I. V. Grigorieva, K. S. Novoselov, L. S. Levitov, and A. K. Geim, Detecting topological currents in graphene superlattices, Science **346**, 448 (2014).
[11] M. Sui, G. Chen, L. Ma, W.-Y. Shan, D. Tian, K. Watanabe, T. Taniguchi, X. Jin, W. Yao, D. Xiao, and Y. Zhang, Gate-tunable topological valley transport in bilayer graphene, Nat. Phys. **11**, 1027 (2015).
[12] Y. Shimazaki, M. Yamamoto, I. V. Borzenets, K. Watanabe, T. Taniguchi, and S. Tarucha, Generation and detection of pure valley current by electrically induced Berry curvature in bilayer graphene, Nat. Phys. **11**, 1032 (2015).
[13] D. Xiao, G.-B. Liu, W. Feng, X. Xu, and W. Yao, Coupled Spin and Valley Physics in Monolayers of MoS_2 and Other Group-VI Dichalcogenides, Phys. Rev. Lett. **108**, 196802 (2012).
[14] K. F. Mak, K. L. McGill, J. Park, and P. L. McEuen, The valley Hall effect in MoS_2 transistors, Science **344**, 1489 (2014).
[15] I. Martin, Y. M. Blanter, and A. F. Morpurgo, Topological Confinement in Bilayer Graphene, Phys. Rev. Lett. **100**, 036804 (2008).
[16] J. Jung, F. Zhang, Z. Qiao, and A. H. MacDonald, Valley-Hall kink and edge states in multilayer graphene, Phys. Rev. B **84**, 075418 (2011).
[17] Z. Qiao, J. Jung, Q. Niu, and A. H. MacDonald, Electronic Highways in Bilayer Graphene, Nano Lett. **11**, 3453 (2011).
[18] A. Vaezi, Y. Liang, D. H. Ngai, L. Yang, and E.-A. Kim, Topological Edge States at a Tilt Boundary in Gated Multilayer Graphene, Phys. Rev. X **3**, 021018 (2013).
[19] F. Zhang, A. H. MacDonald, and E. J. Mele, Valley Chern numbers and boundary modes in gapped bilayer graphene, Proc. Natl. Acad. Sci. **110**, 10546 (2013).
[20] L. Ju, Z. Shi, N. Nair, Y. Lv, C. Jin, J. Velasco Jr, C. Ojeda-Aristizabal, H. A. Bechtel, M. C. Martin, A. Zettl, J. Analytis, and F. Wang, Topological valley transport at bilayer graphene domain walls, Nature **520**, 650 (2015).
[21] J. Li, K. Wang, K. J. McFaul, Z. Zern, Y. Ren, K. Watanabe, T. Taniguchi, Z. Qiao, and J. Zhu, Gate-controlled topological conducting channels in bilayer graphene, Nat. Nanotechnol. **11**, 1060 (2016).
[22] L.-J. Yin, H. Jiang, J.-B. Qiao, and L. He, Direct imaging of topological edge states at a bilayer graphene domain wall, Nat. Commun. **7**, 11760 (2016).
[23] J. Li, R.-X. Zhang, Z. Yin, J. Zhang, K. Watanabe, T. Taniguchi, C. Liu, and J. Zhu, A Valley valve and electron beam splitter, Science **362**, 1149 (2018).
[24] H. Chen, P. Zhou, J. Liu, J. Qiao, B. Oezyilmaz, and J. Martin, Gate controlled valley polarizer in bilayer graphene, Nat. Commun. **11**, 1202 (2020).
[25] G. W. Semenoff, V. Semenoff, and F. Zhou, Domain Walls in Gapped Graphene, Phys. Rev. Lett. **101**, 087204 (2008).
[26] Y. Kim, K. Choi, J. Ihm, and H. Jin, Topological domain walls and quantum valley Hall effects in silicene, Phys. Rev. B **89**, 085429 (2014).
[27] S.-G. Cheng, H. Liu, H. Jiang, Q.-F. Sun, and X. C. Xie, Manipulation and Characterization of the Valley-Polarized Topological Kink States in Graphene-Based Interferometers, Phys. Rev. Lett. **121**, 156801 (2018).
[28] C. Hu, V. Michaud-Rioux, W. Yao, and H. Guo, Moiré Valleytronics: Realizing Dense Arrays of Topological Helical Channels, Phys. Rev. Lett. **121**, 186403 (2018).
[29] Z. Wang, S. Cheng, X. Liu, and H. Jiang, Topological kink states in graphene, Nanotechnology **32**, 402001 (2021).
[30] S.-Q. Shen, *Topological Insulators: Dirac Equation in Condensed Matters* (Springer, Berlin, 2012).
[31] G. Junker, *Supersymmetric Methods in Quantum and Statistical Physics* (Springer, Berlin, 1996).
[32] R. Jackiw and C. Rebbi, Solitons with fermion number 1/2, Phys. Rev. D **13**, 3398 (1976).
[33] W. P. Su, J. R. Schrieffer, and A. J. Heeger, Solitons in Polyacetylene, Phys. Rev. Lett. **42**, 1698 (1979).
[34] I. Adagideli, P. M. Goldbart, A. Shnirman, and A. Yazdani, Low-Energy Quasiparticle States near Extended Scatterers in *d*-Wave Superconductors and Their Connection with SUSY Quantum Mechanics, Phys. Rev. Lett. **83**, 5571 (1999).
[35] K. Sengupta, I. Žutić, H.-J. Kwon, V. M. Yakovenko, and S. Das Sarma, Midgap edge states and pairing symmetry of quasi-one-dimensional organic superconductors, Phys. Rev. B **63**, 144531 (2001).
[36] D.-H. Lee, G.-M. Zhang, and T. Xiang, Edge Solitons of Topological Insulators and Fractionalized Quasiparticles in Two Dimensions, Phys. Rev. Lett. **99**, 196805 (2007).
[37] Y. Nishida, L. Santos, and C. Chamon, Topological superconductors as nonrelativistic limits of Jackiw-Rossi and Jackiw-Rebbi models, Phys. Rev. B **82**, 144513 (2010).
[38] K. Yasuda, M. Mogi, R. Yoshimi, A. Tsukazaki, K. Takahashi, M. Kawasaki, F. Kagawa, and Y. Tokura, Quantized chiral edge conduction on domain walls of a magnetic topological insulator, Science **358**, 1311 (2017).
[39] M. Sedlmayr, N. Sedlmayr, J. Barnaś, and V. Dugaev, Chiral Hall effect in the kink states in topological insulators with mag-

netic domain walls, Phys. Rev. B **101**, 155420 (2020).
[40] H. Pan, Z. Li, C.-C. Liu, G. Zhu, Z. Qiao, and Y. Yao, Valley-polarized Quantum Anomalous Hall Effect in Silicene, Phys. Rev. Lett. **112**, 106802 (2014).
[41] T. Zhou, J. Zhang, B. Zhao, H. Zhang, and Z. Yang, Quantum spin-quantum anomalous Hall insulators and topological transitions in functionalized Sb (111) monolayers, Nano Lett. **15**, 5149 (2015).
[42] T. Zhou, J. Zhang, Y. Xue, B. Zhao, H. Zhang, H. Jiang, and Z. Yang, Quantum spin-quantum anomalous Hall effect with tunable edge states in Sb monolayer-based heterostructures, Phys. Rev. B **94**, 235449 (2016).
[43] J. Zhou, Q. Sun, and P. Jena, Valley-polarized Quantum Anomalous Hall Effect in Ferrimagnetic Honeycomb Lattices, Phys. Rev. Lett. **119**, 046403 (2017).
[44] M. Tahir, A. Manchon, K. Sabeeh, and U. Schwingenschlögl, Quantum spin/valley Hall effect and topological insulator phase transitions in silicene, Appl. Phys. Lett. **102**, 162412 (2013).
[45] H. Huang, Z. Wang, N. Luo, Z. Liu, R. Lü, J. Wu, and W. Duan, Time-reversal symmetry protected chiral interface states between quantum spin and quantum anomalous Hall insulators, Phys. Rev. B **92**, 075138 (2015).
[46] R. Banerjee, S. Mandal, and T. C. H. Liew, Optically induced topological spin-valley Hall effect for exciton polaritons, Phys. Rev. B **103**, L201406 (2021).
[47] X.-L. Qi and S.-C. Zhang, Topological insulators and superconductors, Rev. Mod. Phys. **83**, 1057 (2011).
[48] S. F. Islam and C. Benjamin, A scheme to realize the quantum spin-valley Hall effect in monolayer graphene, Carbon **110**, 304 (2016).
[49] A. Dyrdał and J. Barnaś, Anomalous, spin, and valley Hall effects in graphene deposited on ferromagnetic substrates, 2D Mater. **4**, 034003 (2017).
[50] T. Zhou, J. Zhang, H. Jiang, I. Žutić, and Z. Yang, Giant spin-valley polarizations and multiple Hall effects in functionalized bismuth monolayers, npj Quant. Mater. **3**, 39 (2018).
[51] S. Zhang, S. Guo, Z. Chen, Y. Wang, H. Gao, J. Gómez-Herrero, P. Ares, F. Zamora, Z. Zhu, and H. Zeng, Recent progress in 2D group-VA semiconductors: from theory to experiment, Chem. Soc. Rev. **47**, 982 (2018).
[52] R. Gui, H. Jin, Y. Sun, X. Jiang, and Z. Sun, Two-dimensional group-VA nanomaterials beyond black phosphorus: synthetic methods, properties, functional nanostructures and applications, J. Mater. Chem. A **7**, 25712 (2019).
[53] J. Ji, X. Song, J. Liu, Z. Yan, C. Huo, S. Zhang, M. Su, L. Liao, W. Wang, Z. Ni, Y. Hao, and H. Zeng, Two-dimensional antimonene single crystals grown by van der Waals epitaxy, Nat. Commun. **7**, 13352 (2016).
[54] G. Xu, T. Zhou, B. Scharf, and I. Žutić, Optically Probing Tunable Band Topology in Atomic Monolayers, Phys. Rev. Lett. **125**, 157402 (2020).
[55] Z. Song, C.-C. Liu, J. Yang, J. Han, M. Ye, B. Fu, Y. Yang, Q. Niu, J. Lu, and Y. Yao, Quantum spin Hall insulators and quantum valley Hall insulators of BiX/SbX (X=H, F, Cl and Br) monolayers with a record bulk band gap, NPG Asia Mater. **6**, e147 (2014).
[56] Z. Liu, W. Feng, H. Xin, Y. Gao, P. Liu, Y. Yao, H. Weng, and J. Zhao, Two-dimensional Spin-valley-coupled Dirac Semimetals in Functionalized SbAs Monolayers, Mater. Horiz. **6**, 781 (2019).
[57] S.-S. Li, W.-X. Ji, P. Li, S.-J. Hu, T. Zhou, C.-W. Zhang, and S.-S. Yan, Unconventional band inversion and intrinsic quantum spin Hall effect in functionalized group-V binary films, Sci. Rep. **7**, 6126 (2017).
[58] Y. Ren, Z. Qiao, and Q. Niu, Topological phases in two-dimensional materials: a review, Rep. Prog. Phys. **79**, 066501 (2016).
[59] O. Ávalos-Ovando, D. Mastrogiuseppe, and S. E. Ulloa, Lateral interfaces of transition metal dichalcogenides: A stable tunable one-dimensional physics platform, Phys. Rev. B **99**, 035107 (2019).
[60] H. Pan, X. Li, F. Zhang, and S. A. Yang, Perfect valley filter in a topological domain wall, Phys. Rev. B **92**, 041404 (2015).
[61] S. Das Sarma, S. Adam, E. Hwang, and E. Rossi, Electronic transport in two-dimensional graphene, Rev. Mod. Phys. **83**, 407 (2011).
[62] S. Datta, *Electronic Transport in Mesoscopic Systems* (Cambridge university press, 1997).
[63] M. P. L. Sancho, J. L. Sancho, and J. Rubio, Quick iterative scheme for the calculation of transfer matrices: application to Mo (100), J. Phys. F: Met. Phys. **14**, 1205 (1984).
[64] H. Jiang, L. Wang, Q.-F. Sun, and X. C. Xie, Numerical Study of the Topological Anderson Insulator in HgTe/CdTe Quantum Wells, Phys. Rev. B **80**, 165316 (2009).
[65] Z. Qiao, Y. Han, L. Zhang, K. Wang, X. Deng, H. Jiang, S. A. Yang, J. Wang, and Q. Niu, Anderson Localization from the Berry-Curvature Interchange in Quantum Anomalous Hall Systems, Phys. Rev. Lett. **117**, 056802 (2016).
[66] S.-G. Cheng, R.-Z. Zhang, J. Zhou, H. Jiang, and Q.-F. Sun, Perfect valley filter based on a topological phase in a disordered Sb monolayer heterostructure, Phys. Rev. B **97**, 085420 (2018).
[67] P. W. Anderson, Absence of Diffusion in Certain Random Lattices, Phys. Rev. **109**, 1492 (1958).
[68] C. G. Montgomery, J. I. Krugler, and R. M. Stubbs, Green's-Function Theory of a Disordered Heisenberg Ferromagnet, Phys. Rev. Lett. **25**, 669 (1970).
[69] A. Rycerz, J. Tworzydło, and C. W. J. Beenakker, Anomalously large conductance fluctuations in weakly disordered graphene, Europhys. Lett. **79**, 57003 (2007).
[70] S.-G. Cheng, J. Zhou, H. Jiang, and Q.-F. Sun, The valley filter efficiency of monolayer graphene and bilayer graphene line defect model, New J. Phys. **18**, 103024 (2016).
[71] See Supplemental Material for first-principles calculation methods, fabrication details, expanded discussion of the conductance calculations with disorder, and the influence of the Rashba spin-orbit coupling, temperature and interface configurations, which includes Refs. [72–79].
[72] G. Kresse and J. Furthmüller, Efficient iterative schemes for ab initio total-energy calculations using a plane-wave basis set, Phys. Rev. B **54**, 11169 (1996).
[73] J. P. Perdew, K. Burke, and M. Ernzerhof, Generalized Gradient Approximation Made Simple, Phys. Rev. Lett. **77**, 3865 (1996).
[74] Y. Yao, L. Kleinman, A. MacDonald, J. Sinova, T. Jungwirth, D.-S. Wang, E. Wang, and Q. Niu, First Principles Calculation of Anomalous Hall Conductivity in Ferromagnetic bcc Fe, Phys. Rev. Lett. **92**, 037204 (2004).
[75] Q. Wu, S. Zhang, H.-F. Song, M. Troyer, and A. A. Soluyanov, WannierTools: An open-source software package for novel topological materials, Comput. Phys. Commun. **224**, 405 (2018).
[76] X. Ni, H. Huang, and F. Liu, Robustness of topological insulating phase against vacancy, vacancy cluster, and grain boundary bulk defects, Phys. Rev. B **101**, 125114 (2020).
[77] C. Xu and J. E. Moore, Stability of the quantum spin Hall effect: Effects of interactions, disorder, and Z_2 topology, Phys. Rev. B **73**, 045322 (2006).
[78] J. C. Budich, F. Dolcini, P. Recher, and B. Trauzettel, Phonon-

induced backscattering in helical edge states, Phys. Rev. Lett. **108**, 086602 (2012).

[79] E. S. Walker, S. Muschinske, C. J. Brennan, S. R. Na, T. Trivedi, S. D. March, Y. Sun, T. Yang, A. Yau, D. Jung, A. F. Briggs, E. M. Krivoy, M. L. Lee, K. M. Liechti, E. T. Yu, D. Akinwande, and S. R. Bank, Composition-dependent structural transition in epitaxial $Bi_{1-x}Sb_x$ thin films on Si(111), Phys. Rev. Materials **3**, 064201 (2019).

[80] M. König, S. Wiedmann, C. Brüne, A. Roth, H. Buhmann, L. W. Molenkamp, X.-L. Qi, and S.-C. Zhang, Quantum spin Hall insulator state in HgTe quantum wells, Science **318**, 766 (2007).

[81] D. Culcer, A. Cem Keser, Y. Li, and G. Tkachov, Transport in two-dimensional topological materials: recent developments in experiment and theory, 2D Mater. **7**, 022007 (2020).

[82] G. Li, W. Hanke, E. M. Hankiewicz, F. Reis, J. Schäfer, R. Claessen, C. Wu, and R. Thomale, Theoretical paradigm for the quantum spin Hall effect at high temperatures, Phys. Rev. B **98**, 165146 (2018).

[83] D. Hsieh, D. Qian, L. Wray, Y. Xia, Y. S. Hor, R. J. Cava, and M. Z. Hasan, A topological Dirac insulator in a quantum spin Hall phase, Nature **452**, 970 (2008).

[84] H. Huang, K.-H. Jin, and F. Liu, Alloy Engineering of Topological Semimetal Phase Transition in $MgTa_{2-x}Nb_xN_3$, Phys. Rev. Lett. **120**, 136403 (2018).

[85] P. Schüffelgen, D. Rosenbach, C. Li, T. W. Schmitt, M. Schleenvoigt, A. R. Jalil, S. Schmitt, J. Kölzer, M. Wang, B. Bennemann, U. Parlak, L. Kibkalo, S. Trellenkamp, T. Grap, D. Meertens, M. Luysberg, G. Mussler, E. Berenschot, N. Tas, A. A. Golubov, A. Brinkman, T. Schäpers, and D. Grützmacher, Selective area growth and stencil lithography for in situ fabricated quantum devices, Nat. Nanotechnol. **14**, 825 (2019).

[86] M.-S. Chen, S. L. Brandow, T. L. Schull, D. B. Chrisey, and W. J. Dressick, A Non-Covalent Approach for Depositing Spatially Selective Materials on Surfaces, Adv. Funct. Mater. **15**, 1364 (2005).

[87] H. Dery, Y. Song, P. Li, and I. Žutić, Silicon spin communications, Appl. Phys. Lett. **99**, 121111 (2011).

[88] I. Žutić, A. Matos-Abiague, B. Scharf, H. Dery, and K. Belashchenko, Proximitized materials, Mater. Today **22**, 85 (2019).

[89] M. Lindemann, G. Xu, T. Pusch, R. Michalzik, M. R. Hofmann, I. Žutić, and N. C. Gerhardt, Ultrafast spin-lasers, Nature **568**, 212 (2019).

[90] A. J. Mannix, B. Kiraly, M. C. Hersam, and N. P. Guisinger, Synthesis and chemistry of elemental 2D materials, Nat. Rev. Chem. **1**, 0014 (2017).

[91] Y. Xu, B. Yan, H.-J. Zhang, J. Wang, G. Xu, P. Tang, W. Duan, and S.-C. Zhang, Large-Gap Quantum Spin Hall Insulators in Tin Films, Phys. Rev. Lett. **111**, 136804 (2013).

[92] R. Balog, B. Jørgensen, L. Nilsson, M. Andersen, E. Rienks, M. Bianchi, M. Fanetti, E. Laegsgaard, A. Baraldi, S. Lizzit, Z. Sljivancanin, F. Besenbacher, B. Hammer, T. G. Pedersen, P. Hofmann, and L. Hornekaer, Bandgap opening in graphene induced by patterned hydrogen adsorption, Nat. Mater. **9**, 315 (2010).

[93] F. Karlický, K. Kumara Ramanatha Datta, M. Otyepka, and R. Zbořil, Halogenated Graphenes: Rapidly Growing Family of Graphene Derivatives, ACS Nano **7**, 6434 (2013).

[94] A. Hebard, A. Fiory, and R. Eick, Experimental considerations in the quest for a thin-film superconducting field-effect transistor, IEEE Trans. Magn. **23**, 1279 (1987).

[95] J. Mannhart, J. Ströbel, J. G. Bednorz, and C. Gerber, Large electric field effects in $YBa_2Cu_3O_{7-\delta}$ films containing weak links, Appl. Phys. Lett. **62**, 630 (1993).

[96] L. Fu and C. L. Kane, Superconducting Proximity Effect and Majorana Fermions at the Surface of a Topological Insulator, Phys. Rev. Lett. **100**, 096407 (2008).

[97] I. Adagideli, M. Wimmer, and A. Teker, Effects of electron scattering on the topological properties of nanowires: Majorana fermions from disorder and superlattices, Phys. Rev. B **89**, 144506 (2014).

[98] A. Habibi, S. A. Jafari, and S. Rouhani, Resilience of Majorana fermions in the face of disorder, Phys. Rev. B **98**, 035142 (2018).